applied mechanics

Article

A Simplified Mechanical Model for Rocking Structures on Compliant Foundations

Baojun Yuan [1,*], Mirjam Kloos [2] and Hamid Sadegh-Azar [1]

[1] Institute of Structural Analysis and Dynamics, Department of Civil Engineering, RPTU University Kaiserslautern–Landau, Paul–Ehrlich–Straße 14, 67663 Kaiserslautern, Germany; hamid.sadegh-azar@rptu.de
[2] KOCH Solutions GmbH, Karl–Koch–Straße 1, 66787 Wadgassen, Germany; mgross@rhrk.uni-kl.de
* Correspondence: baojun.yuan@bauing.uni-kl.de

Abstract

Housner's classical rocking model assumes a rigid base, which often leads to inaccurate seismic assessments under real–world soil conditions. This study quantitatively establishes the applicability limits of the rigid–base assumption and defines a reference range for its validity. To address these limitations, a novel soil–structure interaction (SSI) rocking model was developed using Lagrange's formulation, incorporating an event–driven spring–dashpot mechanism to characterize contact forces. Validation against LS–DYNA simulations and existing compliant base models confirms high predictive accuracy across diverse geometries and ground motions. Crucially, an empirical formulation for the interface stiffness of rocking structures was derived to ensure the alignment of the proposed analytical model with numerical observations, thereby enhancing its practical utility in industrial design. Our findings reveal that rocking behavior depends not only on soil stiffness but also on the inherent stiffness of the structure. Specifically, soft soils significantly alter rocking initiation thresholds and amplify peak angles. The proposed SSI–rocking model provides a computationally efficient and FE–compatible tool for optimizing the seismic stability of unanchored structures on flexible foundations.

Keywords: soil–structure interaction (SSI); Rocking dynamics; Lagrange Equation; compliant base

1. Introduction

The seismic resilience of large mobile equipment, including cranes, stacker–reclaimers, and ship loaders, has garnered significant attention in recent years, driven by their increasing prevalence in seismically active regions [1–3]. Unlike conventional fixed structures, these non–anchored systems exhibit unique dynamic characteristics, notably their ability to uplift, tilt, and rock during seismic events. To effectively analyze this rocking behavior, idealizing the equipment as a rigid body provided a simplified yet representative approach. Pioneering work by Housner (1963) established the groundwork for understanding rocking response by examining the behavior of rigid blocks [4]. His research introduced fundamental concepts such as the critical acceleration required to initiate rocking while also revealing the highly nonlinear nature of rocking dynamics. This nonlinearity arose from energy dissipation through impacts and intricate interactions with the supporting ground, underscoring the complexity of accurately predicting the seismic response of such equipment.

Check for updates

Received: 4 March 2026
Revised: 6 May 2026
Accepted: 27 May 2026
Published: 17 June 2026

Copyright: © 2026 by the authors. Licensee MDPI, Basel, Switzerland. This article is an open access article distributed under the terms and conditions of the Creative Commons Attribution (CC BY) license.

Yim, Chopra, and Penzien (1980) extended the analysis to consider the effects of base flexibility, showing that a compliant foundation could significantly alter the rocking response [5]. Their work emphasized the importance of soil–structure interaction (SSI) in predicting the seismic performance of rocking blocks. Further research by Makris and Zhang (2001) investigated the influence of block geometry and aspect ratio on rocking stability [6]. They demonstrated that taller, slender blocks were more susceptible to overturning compared to shorter, wider blocks, providing valuable insights into the geometric parameters that affect rocking dynamics. The role of damping was also scrutinized. El-Gawady et al. (2011) conducted experimental tests on free–rocking blocks with different interface materials, showing that rubber interfaces exhibited the highest energy dissipation due to continuous damping mechanisms, while rigid interfaces like concrete and timber led to discrete energy dissipation patterns [7]. DeJong (2014) introduced the concept of dynamically equivalent rocking structures by deriving approximate equivalence between different rocking systems [8,9]. The study proposed a local linearization approach to estimate errors in modeling multi–block rocking mechanisms, enabling improved seismic response predictions for complex rocking structures [8,9]. Another research team, Vassiliou et al., analyzed the rocking response of structures, focusing on solitary rocking bodies and their self–stabilization potential under seismic excitations [10]. They derived analytical solutions and explored dynamic characteristics to assess stability. Vassiliou et al. (2015, 2016) extended this work by developing analytical and finite element models to incorporate deformation effects in rocking blocks, improving seismic response prediction for both rigid and deformable structures [11,12].

Bachmann et al. (2017, 2019) investigated the dynamics of rocking and rolling structures, focusing on their predictability and response under seismic excitations [13–15]. They analyzed podium structures and rigid uplifting systems, highlighting key parameters influencing stability and overturning mechanisms [13–15]. Lachanas et al. (2022) analyzed the influence of the vertical component of ground motion on rocking structures, showing that it significantly altered overturning probabilities and energy dissipation [16]. Reggiani Manzo et al. (2019, 2022) proposed displacement–based analysis methods and developed uniform risk spectra for rocking structures, providing a probabilistic framework to assess their seismic reliability [17,18]. Sieber et al. (2020) examined the robustness of simplified analysis methods for rocking structures, comparing them against detailed numerical simulations to identify limitations in existing predictive models [19]. Kazantzi et al. (2021) presented seismic response distribution expressions for rocking structures, offering probabilistic models for overturning risk assessment [20]. Lachanas et al. (2021, 2022) introduced rocking incremental dynamic analysis and statistical parameterization techniques to quantify rocking response variability under seismic excitation [21,22]. Their findings improved fragility assessment and performance–based seismic evaluation.

Beyond rocking on rigid foundations, recent studies explored how base compliance could critically alter the observed rocking response, necessitating more sophisticated analytical models. Palmeri et al. (2008) conducted a response analysis of rigid structures rocking on flexible foundations, demonstrating how soil–structure interaction modified fundamental rocking behavior [23]. They proposed a simplified approach to account for base compliance in seismic assessments. Vassiliou et al. (2011) analyzed the rocking response of rigid blocks on an isolation base, concluding that seismic isolation removed the beneficial property of increasing stability as block size increased or excitation pulse period decreased [24]. Pelekis et al. (2018, 2019) investigated the seismic behavior of buildings with structural and foundation rocking, emphasizing the interaction between soil and rocking motion [25,26]. They showed that the relative density of sand did not influence structural rocking. Buildings with structural rocking experienced reduced base shear and

floor accelerations compared to fixed–base structures. Their findings emphasized that well–designed structural rocking could enhance seismic resilience by limiting inelastic deformations and reducing overall damage. Lu et al. (2021) developed an improved Winkler–based rocking foundation model that incorporated biaxial hysteretic soil behavior to better capture rocking isolation effects [27]. They found that sliding due to coupled shear-compressive soil behavior tended to reduce the free-vibrational rocking response of blocks with smaller slenderness ratios, while it could either increase or decrease seismic overturning potential of blocks on heavily loaded foundations [27]. He et al. extended the rigid rocking block model with a Winkler foundation to consider the flexibility of the foundation [28]. The study found that damping enhanced overturning resistance, while soil stiffness significantly influenced taller structures. Frost et al. (2023) investigated the dynamic response of rectangular rigid blocks standing on a horizontally moving compliant base, combining analytical, numerical, and experimental approaches [29]. By modeling the impact between the block and the moving base with a series of springs and dampers, the study highlighted the enhanced predictive capabilities of the compliant base model over traditional rigid base models in predicting the initiation of rocking and overall seismic response.

While the research by Frost et al. (2023) [29] highlights the specialized benefits of utilizing base uplift as a seismic isolation mechanism, other contemporary studies explore broader applications of soil–structure interaction (SSI) where the primary objective is preventing disconnection or isolating vibrations through ground modification. Unlike rocking systems that leverage controlled instability, the following research focuses on enhancing structural resilience through conformable buried systems and passive wave barriers. Li et al. (2026) focused on submerged segmental tunnels designed as flexible systems that must strictly conform to ground deformation to maintain a watertight seal [30]. Rasa and Budak (2026) explored soil–structure–trench interaction (SSTI), evaluating the efficacy of open and infilled trenches as barriers to isolate multi–story buildings from localized and seismic ground–borne vibrations [31]. Feng et al. (2025) investigated the dynamic fracture mechanics of twin tunnels, treating the interface between the tunnel and rock as a site of potential failure that must be reinforced to prevent disconnection [32].

It is imperative to note that while these recent studies share a common reliance on soil–mechanical principles, structural rocking on a compliant base represents a fundamentally distinct phenomenon. The dynamic behavior of unanchored, large–scale industrial assets follows a fundamentally different physical logic [2,3]. Unlike embedded systems, the seismic response of structures such as bucket wheel reclaimers and heavy cranes is primarily driven by a “disconnection” mechanism at the contact interface rather than continuous soil coupling. In these systems, energy dissipation is dictated by an “event–driven” contact–impact process at the interface, where the structural body acts as a rigid or semi–rigid entity pivoting on its support. Therefore, this research proposes a new integrated SSI–rocking model and investigates the applicability limits of the classical Housner rocking formulation when soil flexibility and damping are considered.

2. The Applicability Limits of Housner’s Rocking Block Model

Housner’s rocking block model (Figure 1) provides a fundamental framework for analyzing the seismic behavior of unanchored structures, assuming a rigid block on a perfectly rigid base where rocking occurs about fixed pivot points without sliding. The model neglects any internal deformation, treating the structure as a pure rigid body, and considers energy dissipation only through impact when the block switches pivot points. Overturning is defined by exceeding a critical rocking angle, determined by the block’s geometry and seismic excitation, without accounting for foundation flexibility or soil

damping effects. The angular rotation can be computed by solving nonlinear ordinary differential equations:

$$\ddot{\theta}(t) = -\rho^2 \left\{ \sin(\alpha \cdot \mathrm{sgn}(\theta(t)) - \theta(t)) + \frac{\ddot{u}_g(t)}{g} \cos(\alpha \cdot \mathrm{sgn}(\theta(t)) - \theta(t)) \right\} \quad (1)$$

where α represents the slenderness angle of the block which was computed by width and length of the block:

$$\alpha = \tan^{-1}\left(\frac{b}{h}\right) \quad (2)$$

where ρ is the frequency parameter of the rocking block:

$$\rho = \sqrt{\frac{3g}{4R}} \quad (3)$$

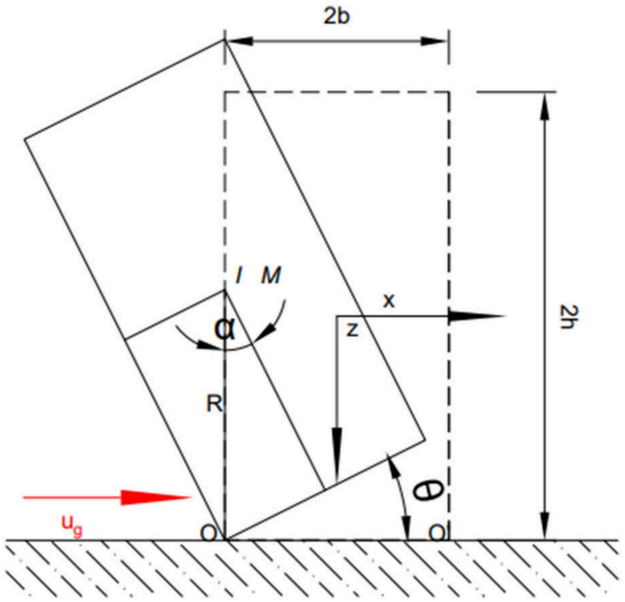


Figure 1. Housner's rocking block model.

The condition to initiate rocking for the rigid block model is determined by the peak ground acceleration (PGA) threshold, where the horizontal ground acceleration exceeds the block's static stability limit.

$$a_g > g tan\alpha \quad (4)$$

During pure rocking, where no sliding or bouncing occurs, the kinetic energy dissipates during each impact to the base. This kinetic energy loss can be treated with coefficient restitution. The relationship of the angular velocities before and after impact gives:

$$r = \frac{\dot{\theta}_2}{\dot{\theta}_1} \quad (5)$$

The formula, that defines the upper bound for the coefficient of restitution of a rigid rocking block, based on angular momentum conservation before and after impact, is given by [4]:

$$r = 1 - \frac{3}{2} sin^2(\alpha) \quad (6)$$

The classical Housner rocking model, which neglects soil flexibility, was evaluated through detailed numerical simulations using the LS–DYNA R14.1.1 explicit solver to explicitly model realistic base conditions and quantify the limitations of this simplification, while also assessing rocking motion and soil–structure interaction (SSI) under varying soil conditions. The numerical model, as depicted in Figure 2, provides a simplified two–dimensional representation of a block–soil system, designed for validation by comparing results against analytical predictions. This model comprises a rigid superstructure, represented by a red rectangular block symbolizing a non–building structure or column, and a blue rectangular base denoting the underlying soil or foundation. Both the block and soil components were modeled using elastic material properties. The rocking motion was simulated by implementing the keyword CONTACT_2D_AUTOMATIC_SURFACE_TO_SURFACE, enabling accurate representation of the dynamic interaction between the block and the base. To further delineate the applicability limits of the Housner model, a parametric study was performed by systematically varying the soil properties.

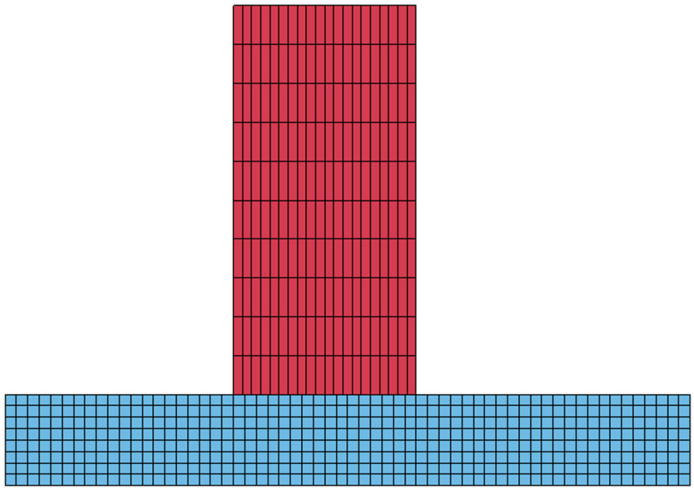


Figure 2. The numerical model in LS–DYNA: the rigid block is shown in red, and the soil is shown in blue.

The underlying soil was characterized by using representative soil parameters, including soil density ρ, shear modulus G_{max} and Poisson's ratio μ and dynamic stiffness modulus E_d, as summarized in Table 1. The relationship between the dynamic shear modulus and dynamic elastic modulus is defined as [33]:

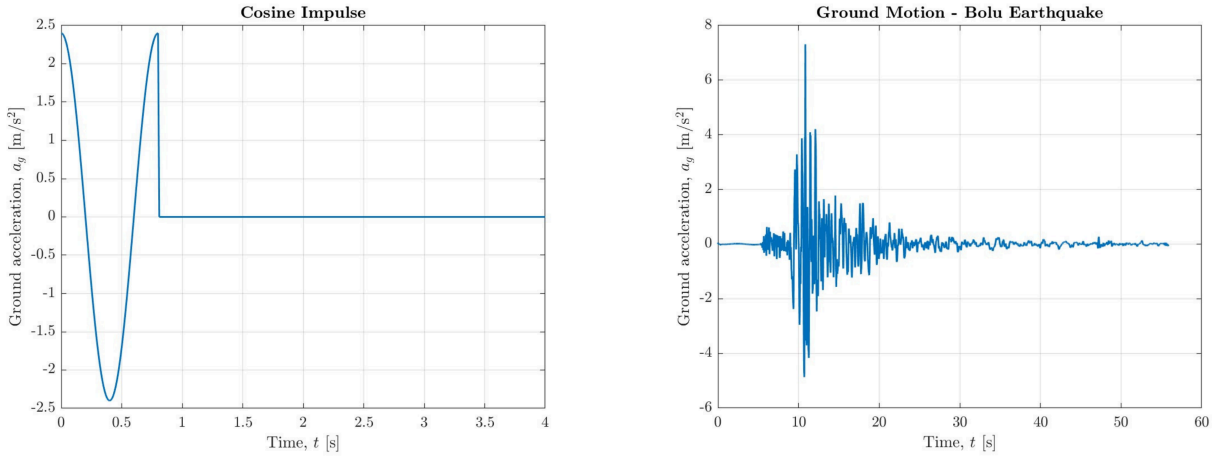
$$E_d = G_d \frac{2(1-\mu)}{1-2\mu} \tag{7}$$

Table 1. Soil properties for modelling compliant base.

Ground Type	Density ρ (kg/m^3)	Dynamic Shear Modulus G_{max} (MN/m^2)	Poisson's Ratio μ	Dynamic Elastic Modulus E_d (MN/m^2)
Sand	1900	80	0.3	280
Gravel	2000	300	0.3	1050
Rock	2500	1000	0.3	3500
Steel	7800	80,000	0.3	210,000

The selected soil ranged broadly from very soft (clay) to highly stiff (rock) and nearly rigid (steel) enabling a comprehensive assessment of soil compliance impacts on rocking behavior. For each soil configuration, the numerical rocking response of the rigid block under seismic loading was compared directly with the analytical solution from Housner's model. By evaluating discrepancies between results from the numerical simulation and Housner's model, we clearly identified a critical stiffness threshold below which Housner's model predictions become unreliable. This threshold is defined by a shear modulus ranging from 300 to 1000 MPa.

The subsequent investigation, underpinned by LS–DYNA simulations under both cosine function and earthquake excitation tests (as illustrated in Figure 3), revealed critical insights into the applicability of Housner's model. The model exhibited a relatively robust agreement with the predicted rocking motion on rigid bases, such as steel (E = 210,000 MPa) and rock (G = 1000 MPa). However, as the soil stiffness diminished, particularly when the shear modulus fell below 300 MPa, the Housner model's assumptions of a rigid base proved inadequate, rendering it inapplicable for accurately predicting rocking behavior on softer soil substrates. In addition, simulations show a sharp increase in the maximum rocking angle on clay compared to other soil types.



(**a**) (**b**)

Figure 3. Cosine excitation and Turkey Bolu earthquake ground motion.

The criterion for initiating rocking motion is significantly altered when soil flexibility is considered, as demonstrated in Figure 4a,c,e,g. While Housner's classical model predicts no rocking motion under cosine excitation due to its rigid–base assumption, the LS–DYNA simulations reveal that rocking is indeed initiated, driven by the compliant nature of the soil base. Moreover, the simulations indicate that the softer the soil, the larger the rocking motion could become, owing to increased base compliance and reduced effective stiffness. This phenomenon is also presented in Figure 4b,d,f,h. This discrepancy underscores the limitations of Housner's formulation in capturing soil–structure interaction effects, highlighting the imperative need to develop an enhanced rocking model that explicitly accounts for the dynamics of a compliant base to accurately predict rocking behavior under such conditions. To quantitatively assess the discrepancies inherent in the classical Housner model, this study employs the normalized root mean square error (NRMSE) and relative peak error (RPE) as a primary metric for performance evaluation.

$$NRMSE = \frac{\sqrt{\frac{1}{n}\sum_{i=1}^{n}[\theta_{LS}(t_i) - \theta_H(t_i)]^2}}{\theta_{max,LS}} \times 100\% \quad (8)$$

where $\theta_{LS}(t_i)$ is the rotation angle predicted by the LS–DYNA simulation at time step i, $\theta_H(t_i)$ is the rotation angle predicted by the classical Housner model at time step i, and $\theta_{max,LS}$ is the maximum of the rotation angle predicted by the LS–DYNA simulation. Since the stability and potential overturning of unanchored structures are often governed by the maximum tilt angle, the relative peak error (RPE) is also used for performance evaluation.

$$RPE = \left| \frac{\theta_{max,LS} - \theta_{max,H}}{\theta_{max,LS}} \right| \times 100\% \quad (9)$$

where $\theta_{max,LS}$ is the maximum rotation angle predicted by the LS–DYNA simulation and $\theta_{max,H}$ is the maximum rotation angle predicted by the classical Housner model.

Figure 5a shows a 100% relative peak error across all soil types. This suggests that for this specific excitation, the classical Housner model fails to capture the peak rocking amplitude entirely due to the initialization condition of rocking, which leads to a massive discrepancy in the predicted maximum rotation. Figure 5b clearly shows the dependency on soil stiffness. The relative peak error is significantly higher for soft soils such as clay and sand, exceeding 60% and falling well above the 10% accuracy threshold. However, as base stiffness increases (e.g., rock and steel), the error decreases substantially, with rock and steel falling well within the acceptable 10% limit. Consequently, a dynamic shear modulus of 1000 MPa (characteristic of rock) is established as an approximate upper bound for the applicability of Housner's model. Below this threshold, the predictive accuracy of the model degrades significantly, failing to yield reliable structural rocking responses. However, in this case, the NRMSE metric, as shown in Figure 5c,d, becomes statistically diluted and fails to reflect the true magnitude of the predictive failure.

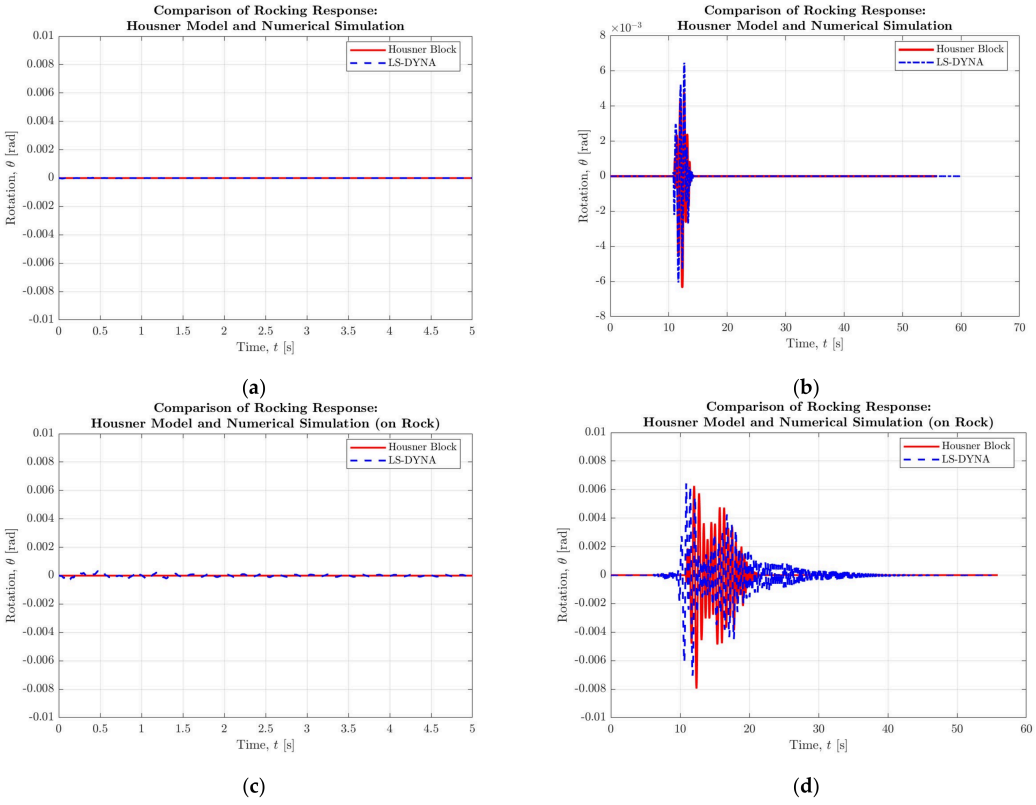


Figure 4. *Cont.*

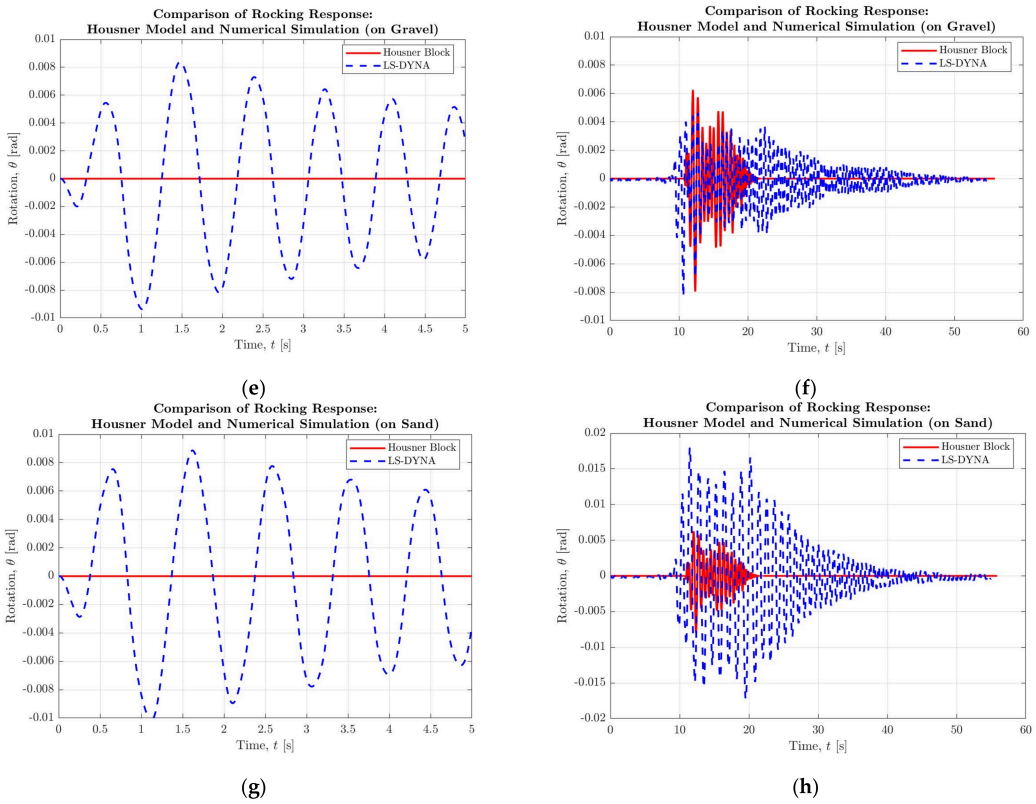


Figure 4. Comparison of the Housner model and LS–DYNA simulations for rigid block rocking under cosine and earthquake excitations. Results are shown for four base materials: (**a**,**b**) steel (E = 210,000 MPa), (**c**,**d**) rock (G = 1000 MPa), (**e**,**f**) gravel (G = 300 MPa), and (**g**,**h**) sand (G = 80 MPa).

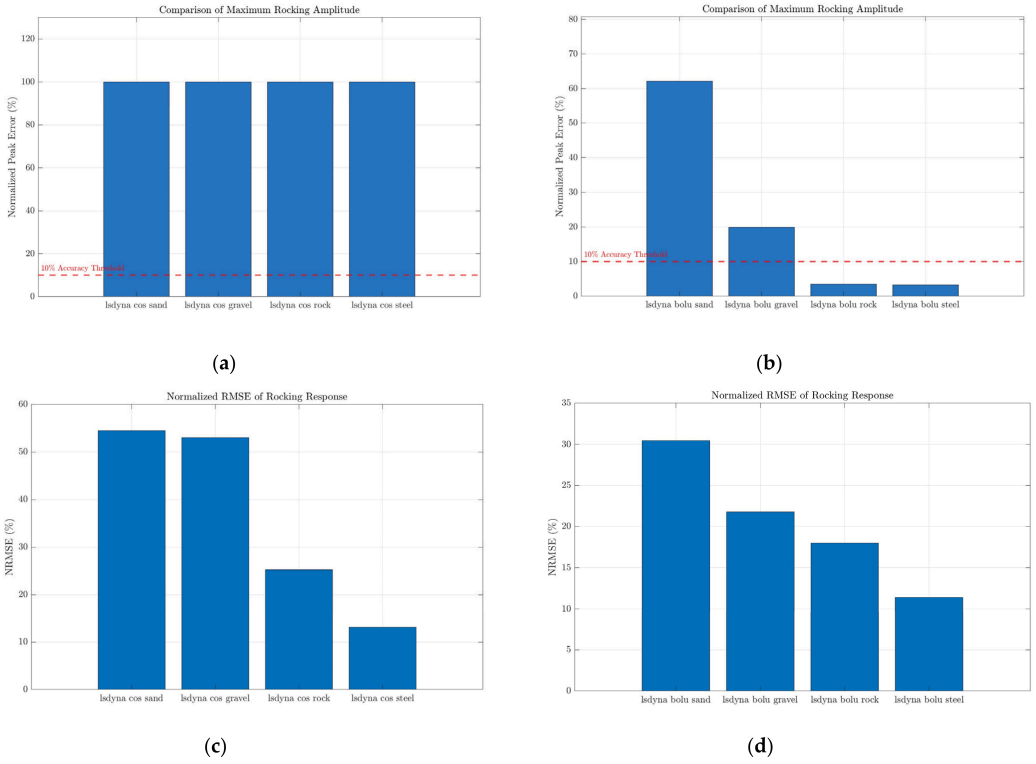


Figure 5. The normalized peak error (RPE) and normalized root mean square error (NRMSE) (Figure 5) of Housner's model were calculated for predicting the rocking response under various ground conditions (sand, gravel, rock and steel) and different seismic excitations. (**a**,**b**) under cosine excitation; (**c**,**d**) under Bolu earthquake excitation.

3. Development of a Novel SSI–Rocking Model for a Non–Anchored Structure on a Compliant Base

In real–world scenarios, soil compliance plays a crucial role in structural rocking. A compliant base introduces additional vertical and rotational compliance, damping effects, and energy dissipation mechanisms, which can either enhance or impair stability. Experimental and numerical studies have shown that neglecting soil flexibility can lead to significant errors in predicting the overturning threshold and energy dissipation [23,27].

To address these limitations, we propose a novel SSI–rocking model that explicitly incorporates the elastic and damping properties of the soil. As shown in Figure 6, the model is formulated using the Lagrange method to capture the rocking behavior of structures on compliant foundations, improving upon classic rocking models by accounting for base flexibility. The proposed SSI–rocking model considers a two degree of freedom (2–DOF) system subjected to ground excitation, where the structure's mass is idealized at its center. The system includes both rotational motion θ and translational motion to simulate base compliance effects. The base is modeled using frequency–dependent stiffness and damping characteristics, denoted as $K_v(\Omega)$ and $C_v(\Omega)$, respectively. The stiffness considers the soil flexibility and the contact stiffness between blocks and the base. Energy dissipation due to inelastic impacts at the rocking edges is captured through an equivalent viscous damper, implemented as a dashpot. Unlike Housner's model, where damping occurs discontinuously only at the instant of impact, the proposed model features a viscous damper that operates continuously throughout the motion. Additionally, no plasticity or permanent deformation of the soil is considered. The Lagrange formulation is used to derive the equations of motion, incorporating both conservative forces, such as gravity and elastic restoring forces, and non–conservative effects, including damping and impact–induced energy losses.

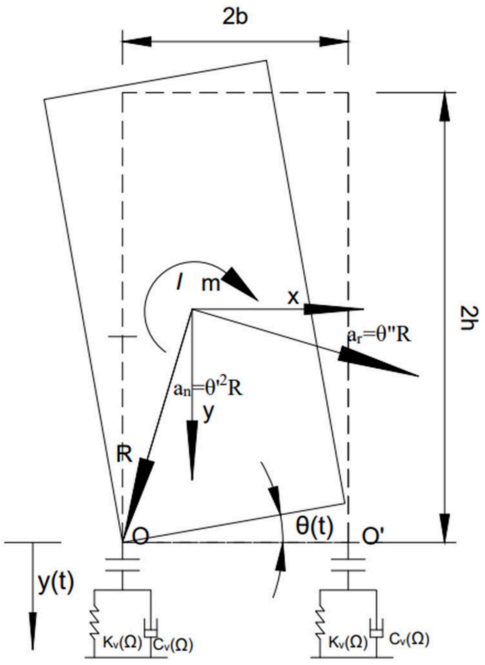


Figure 6. The rocking block model on compliant base.

The rotational and vertical contributions to the system's kinetic energy are:

$$E_k = \frac{1}{2}I\dot{\theta}^2 + \frac{1}{2}m\left[\dot{y} + Rsin(\alpha sgn(\theta) - \theta)\dot{\theta}\right]^2 \quad (10)$$

The potential energy of the system is given, where the zero potential energy surface was defined at the pivot point of the rocking block.

$$E_p = \frac{1}{2}ky^2 + mg[Rcos(\alpha sgn(\theta) - \theta) - y] \tag{11}$$

For non–conservative rocking system on compliant base, the Lagrange equation gives

$$\begin{array}{c} \frac{d}{dt}\left(\frac{\partial L}{\partial \dot{\theta}}\right) - \frac{\partial L}{\partial \theta} = Q(t) \\ \frac{d}{dt}\left(\frac{\partial L}{\partial \dot{y}}\right) - \frac{\partial L}{\partial y} = -c\dot{y} \end{array} \tag{12}$$

The interface stiffness and damping properties are defined as follows:

$$k = m\omega^2, c = 2m\omega\xi \tag{13}$$

where ω represents the natural frequency of the equivalent spring, ξ represents the damping ratio. Combining Equations (10)–(12), the Lagrange Equations are simplified as follows:

$$\left(I + mR^2\right)\ddot{\theta} - mR^2\ddot{y}\sin(A) + mgRsin(A) = -m\ddot{u}_g Rcos(A) \tag{14}$$

$$m\ddot{y} - mR\ddot{\theta}\, sin(A) + mR\dot{\theta}^2 cos(A) - mg = -F_C \tag{15}$$

with the following quantities:

$$A(t) = sgn(\theta(t))\alpha - \theta(t), \quad I = \frac{4}{3}mR^2 \tag{16}$$

To mathematically define the transition between contact states, the interface is modeled using a gap element that distinguishes between the full–contact and rocking phases. The contact force F_C is governed by a piecewise function that captures the "event–driven" nature of the interaction. In the non–uplifting phase ($bsin(|\theta|) \leq y_{stat}$), the structure remains in full contact with the compliant base, engaging two sets of spring–dashpot elements to provide maximum resistance. Conversely, during the rocking phase ($bsin(|\theta|) > y_{stat}$) physical uplift occurs, causing a partial disconnection where only one spring–dashpot set remains active to provide the restoring force.

$$F_C = \begin{cases} ky + c\dot{y} & bsin(|\theta|) > y_{stat} \\ 2ky + 2c\dot{y} & bsin(|\theta|) \leq y_{stat} \end{cases} \tag{17}$$

where y_{stat} is the static displacement of the block due to self–weight, it is defined as initial condition by solving the differential Equations (14) and (15).

$$y_{stat} = \frac{mg}{2bk} \tag{18}$$

Combining Equations (14)–(16), the equation of motion of the rocking system on compliant base is derived:

$$\ddot{y}(t) = \frac{\left(g - \omega^2 y - 2\omega\xi\dot{y} - Rcos(A)\dot{\theta}^2 + \frac{3}{7}\left(-\ddot{u}_g cos(A)sin(A) + gsin(A)^2\right)\right)}{\left(1 - \frac{3}{7} * \sin^2(A)\right)} \tag{19}$$

$$\begin{aligned} \ddot{\theta}(t) = \frac{3}{7R}\Bigg\{ \Bigg(\Bigg(g - \omega^2 y - 2\omega\xi\dot{y} - Rcos(A)\dot{\theta}^2 + \frac{3}{7}\left(-\ddot{u}_g cos(A)sin(A) + gsin(A)^2\right)\Bigg)\left(1 - \frac{3}{7} * \sin^2(A)\right)\Bigg)\sin(A) \\ -gsin(A) - \ddot{u}_g\cos(A)\Bigg\} \end{aligned} \tag{20}$$

Equations (19) and (20) can be solved numerically in MATLAB 2024a using ODE45.

4. Numerical Validation and Implementation

To validate the proposed analytical SSI–rocking model, high–fidelity numerical simulations were conducted using LS–DYNA. Beyond finite–element analysis, the model's performance was further compared with the Frost–Winkler Foundation model [29] to ensure a robust comparison across different modelling paradigms. A systematic calibration procedure was employed to optimize the interface stiffness parameters, harmonizing the analytical predictions with the numerical reference data. To ensure a rigorous evaluation, the optimization process was governed by three distinct statistical metrics: the Pearson Correlation Coefficient (PCC), the normalized root mean square error (NRMSE), and the relative peak error (RPE). By integrating these metrics, the calibration simultaneously accounts for linear correlation, global deviation, and the accuracy of local extrema. Consequently, the objective function for the PCC optimization is defined as:

$$\theta^* = \arg\max_{\theta} \operatorname{corr}\left(y^{LS}(t,\theta), y^{\text{model}}(t,\theta)\right) \tag{21}$$

where $y^{\text{LS}}(t)$ represents the rotation time history from the LS–DYNA numerical simulation and $y^{\text{model}}(t,\theta)$ denotes the rocking angle computed by the SSI–rocking model. The correlation coefficient used for calibration is calculated as:

$$\operatorname{corr}\left(y^{\text{ref}}, y^{\text{model}}\right) = \frac{\sum_{i=1}^{N}\left(y_i^{LS} - \overline{y^{LS}}\right)\left(y_i^{\text{model}} - \overline{y^{\text{model}}}\right)}{\sqrt{\sum_{i=1}^{N}\left(y_i^{LS} - \overline{y^{LS}}\right)^2} \cdot \sqrt{\sum_{i=1}^{N}\left(y_i^{\text{model}} - \overline{y^{\text{model}}}\right)^2}} \tag{22}$$

where $\overline{y^{\text{LS}}}$ and $\overline{y^{\text{model}}}$ are the mean values of the LS–DYNA reference data and estimated data from the proposed model, respectively, and N is the number of data points. The optimization function of NRMSE and RPE are expressed as:

$$\theta^* = \arg\min_{\theta} NRMSE\left(y^{LS}(t,\theta), y^{\text{model}}(t,\theta)\right) \tag{23}$$

$$\theta^* = \arg\min_{\theta} RPE\left(y^{LS}(t,\theta), y^{\text{model}}(t,\theta)\right) \tag{24}$$

where NRMSE and RPE are defined in Equations (8) and (9).

To calibrate the proposed model, a grid search was conducted over interface stiffness k values ranging from 1×10^4 to 1×10^6 kN/m, with an equivalent damping ratio ξ ranging from 1% to 7%. These values are applicable to the rocking simulation on sand. For each interface stiffness k, the rocking motion was solved using the ODE45 solver, and the resulting $y^{\text{model}}(t,\theta)$ was compared to the simulation data $y^{\text{LS}}(t)$ to compute the correlation. The interface stiffness k that yielded the highest PCC, lowest NRMSE or lowest RPE was selected to ensure that the analytical model accurately captured the observed dynamic rocking behavior in the numerical simulation. The close agreement between the calibrated analytical solution and the LS–DYNA numerical simulation demonstrates the robustness of the proposed SSI–rocking model for predicting soil–structure interaction dynamics.

Table 2 outlines the calibrated geometry and contact surface parameters utilized for the investigation on sand, distinguishing between two primary structural configurations: a Bulky (SG1) block and a Slender (SG2) block. The geometric properties are defined by widths of 8 m and 6 m, and heights of 17 m and 30 m, respectively. Furthermore, the table details the interface stiffness and damping ratio parameters calibrated under three distinct loading scenarios: Cosine, Turkey Bolu, and El–Centro. Turkey Bolu and

El–Centro are strong motions. These values illustrate how the contact mechanics are tuned to specific excitation types, with interface stiffness values ranging from 2×10^4 kN/m to 7×10^5 kN/m, and damping ratios varying between 1% and 5% depending on the block type and ground motion characteristics.

Table 2. Calibrated geometry and contact surface parameters on sand.

Block Type	Width B (m)	Height H (m)	Interface Stiffness (kN/m)			Damping Ratio (%)		
			Cosine	Turkey Bolu	El–Centro	Cosine	Turkey Bolu	El–Centro
Bulky (SG1)	8	17	7×10^5	3×10^5	7×10^5	1	5	5
Slender (SG2)	6	30	5×10^4	2×10^4	3×10^5	1	3	3

Figure 7 and Tables 3–5 illustrate the seismic rocking responses of a bulky block (SG1) and a slender block (SG2), comparing the results from the proposed SSI–rocking model, Frost's compliant base model, Housner's classical model, and LS–DYNA simulations. Under cosine excitation (Figure 7a,b), Housner's model yields completely unrealistic results because it fails to account for how soft ground, such as sand, alters rocking initiation. Both the proposed and Frost's models show similar predictive accuracy for SG1, each maintaining a NRMSE of approximately 11% compared to the LS–DYNA benchmark. For SG2, the proposed model achieves a higher PCC of 83% and a NRMSE of 29% with less phase mismatch, whereas Frost's model exhibits a lower RPE of about 20% but suffers from greater phase lag.

Table 3. Evaluation for the rocking prediction under cosine excitation.

Configuration	Model	Pearson Correlation Coefficient (%)	NRMSE (%)	RPE (%)
Bulky (SG1)	Housner	0	29.09	100
	Frost	92	11.47	16.82
	Proposed	95	11.15	19.97
Slender (SG2)	Housner	0	29.97	100
	Frost	7	40.14	20.48
	Proposed	83	29.82	111

Table 4. Evaluation for the rocking prediction under Bolu earthquake.

Configuration	Model	Pearson Correlation Coefficient (%)	NRMSE (%)	RPE (%)
Bulky (SG1)	Housner	1.02	15.77	61.98
	Frost	64.9	11.84	34.88
	Proposed	47.02	17.40	22.24
Slender (SG2)	Housner	1.74	13.65	60.68
	Frost	1.58	14.00	52.78
	Proposed	32.7	13.13	47.27

During the Turkey Bolu excitation (Figure 7c,d), Housner's model consistently underestimates the peak rocking response. In this scenario, the proposed model slightly outperforms Frost's model, yielding an RPE of 22% for SG1 and 47% for SG2. Finally, under the El–Centro excitation (Figure 7e,f), the proposed and Frost's models perform similarly for SG1. However, for SG2, the proposed model significantly outperforms the Frost model, achieving a precise RPE of roughly 3% compared to Frost's 30%.

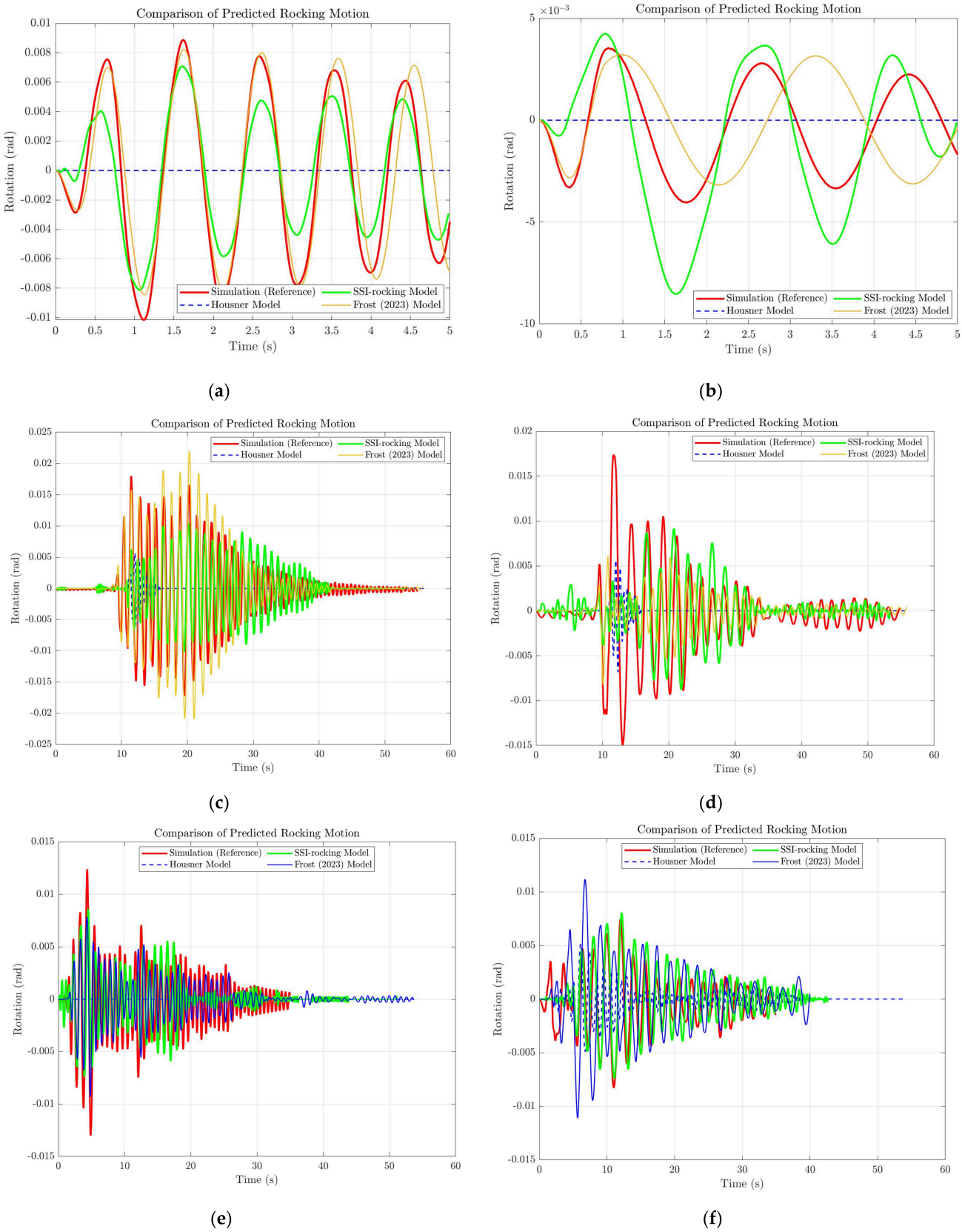


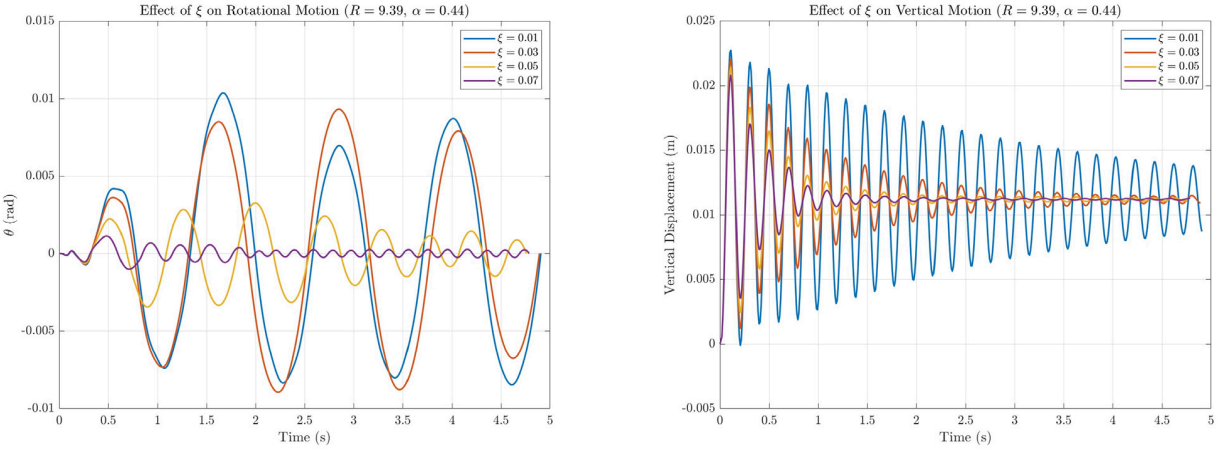
Figure 7. Comparison between LS–DYNA simulation, Housner's model, Frost's model and proposed rocking–SSI model on sand under different excittaions: (**a**) SG1 under cosine excitaiton (**b**) SG2 under cosine excitation (**c**) SG1 under Bolu earthquake (**d**) SG3 under Bolu earthquake (**e**) SG1 under El Centro earthquake (**f**) SG3 under El Centro earthquake.

Table 5. Evaluation for the rocking prediction under El–Centro earthquake.

Configuration	Model	Pearson Correlation Coefficient (%)	NRMSE (%)	RPE (%)
Bulky (SG1)	Housner	0	100	100
	Frost	27.6	13.54	28.26
	Proposed	33	13.46	34.13
Slender (SG2)	Housner	3.4	18.57	37.94
	Frost	25	30.71	34.65
	Proposed	71	13.81	2.97

Ultimately, these results demonstrate that accounting for soil flexibility is essential for accurate seismic assessment. While Housner's model substantially underpredicts oscillation amplitudes due to its rigid–base assumption, the proposed analytical model exhibits close alignment with high–fidelity numerical simulations and yields predictions comparable to the compliant base model by Frost (2023) [29]. However, a key distinction lies in the implementation of these models: while both require the tuning of interface stiffness to match numerical or experimental benchmarks, the proposed SSI model provides a predictive formula (Equation (25)) for this parameter, whereas the Frost model relies on experimental calibration.

This investigation (Figure 8) explores the influence of varying equivalent damping ratios ξ on the dynamic behavior of a rocking structure under controlled conditions ($R = 9.39$, $\alpha = 0.44$). As shown in the left in Figure 8, which depicts the rotational motion under cosine excitation, higher damping ratios markedly enhance the decay rate of oscillations. Notably, $\xi = 0.07$ demonstrates the most significant amplitude reduction, whereas $\xi = 0.01$ sustains larger oscillations over a prolonged duration. Based on these observations, an equivalent damping ratio below 5% is recommended as an optimal threshold for the proposed SSI–rocking model on sand to maintain realistic response characteristics. The right chart in Figure 8 illustrates vertical displacement over the same period, where an increase in damping similarly diminishes vertical motion amplitudes and expedites stabilization. Overall, while the equivalent damping ratio effectively suppresses the magnitude and duration of the response, the system's underlying rocking dynamics are governed more significantly by the interface stiffness than by the damping ratio.



(**a**) (**b**)

Figure 8. Damping influence on rotational (**a**) and vertical (**b**) motion of a block SG1 with stiffness (k = 5 × 10^5 kN/m) and varying equivalent damping ratios (ξ, = 0.01, 0.03, 0.05, 0.07).

5. Empirical Formulation of Interface Stiffness for Rocking Motion

The interface stiffness of a rocking system is physically governed by the interaction between material properties and geometric constraints. The Young's modulus of the block and the shear modulus of the soil define the elastic resistance of the materials to compressive and shear stresses, respectively. The contact area determines the spatial distribution of the rocking load, while the effective depth of the soil domain establishes the volume of material subjected to deformation. Together, these parameters dictate the interface stiffness, which is the dominant factor in controlling the dynamics of rocking motion. To establish a practical relationship for the proposed SSI–rocking model, we analyze the combination of these factors to account for the simultaneous deformability of both the structural block and its supporting foundation.

The proposed stiffness relationship is formulated based on the concept of two elastic bodies in contact, where the overall response is determined by the harmonic sum of their respective stiffness contributions. The rocking effective interface stiffness k is expressed as:

$$k_{interface} = \beta \frac{A}{H} \left[\frac{1}{\frac{1}{G_s} + \frac{1}{E_b}} \right]^n \tag{25}$$

where, G_s represents the dynamic shear modulus of the soil and, E_b is the Young's modulus of the block. The term inside the brackets accounts for the combined compliance of both materials, treating the interface as a system of two springs in series. The fraction form reflects the inverse sum of their individual stiffness contributions, ensuring that the resulting stiffness captures both the flexibility of the soil and the rigidity of the block. The interface area A controls the distribution of contact stress between the block and the soil, H represents the depth of the soil layer that actively participates in the deformation process, effectively controlling the extent of the soil domain that contributes to the rocking response. A deeper soil domain implies a more compliant foundation, reducing the overall rocking stiffness. The ratio $\frac{A}{H}$ thus serves as a geometric scaling factor, while the empirical coefficient β and n are used for the calibration of this empirical formulation. However, the scenario involving multi–layer soil is not studied in this paper.

To rigorously validate the proposed empirical formulation to the interface stiffness, verification data were gathered utilizing four distinct block geometries, each subjected to the three seismic ground motions employed throughout this study. By employing a nonlinear power–law regression, the relationship is characterized by the expression $k = 145.93 \cdot X^{1.59}$, as defined in Equation (25). While internal data variance is observed within the clusters, we noticed the vertical dispersion within the SG1 and SG2 datasets, this scatter is attributed to the inherent stochastic nature of the rocking simulations. Despite these local fluctuations, the regression curve successfully captures the fundamental physical trajectory of the system across the geometric domain. Furthermore, although the empirical validation (Figure 9) was conducted on sandy soil, the model treats the soil domain exclusively within the linear elastic range; consequently, this formulation is considered practically applicable to a scenario governed by elastic soil behavior.

5.1. Influence of Soil Dynamic Shear Modulus G_s

Figure 10 illustrates the rocking response of a block subjected to different soil conditions, characterized by the varying elastic dynamic modulus (E_d). The cosine function (Figure 3) was used as input excitation. The results highlight the influence of soil stiffness on the rocking motion, with softer soils (e.g., clay, $E_d = 130$ MPa) exhibiting greater amplitudes and prolonged oscillations, and stiffer materials (e.g., steel, $E = 210,000$ MPa) significantly suppress rocking motion. This trend indicates that higher soil stiffness increases energy

dissipation and reduces dynamic amplification effects. The observed phase shifts between various soil types provide additional evidence that the rocking period increases as subsoil stiffness decreases.

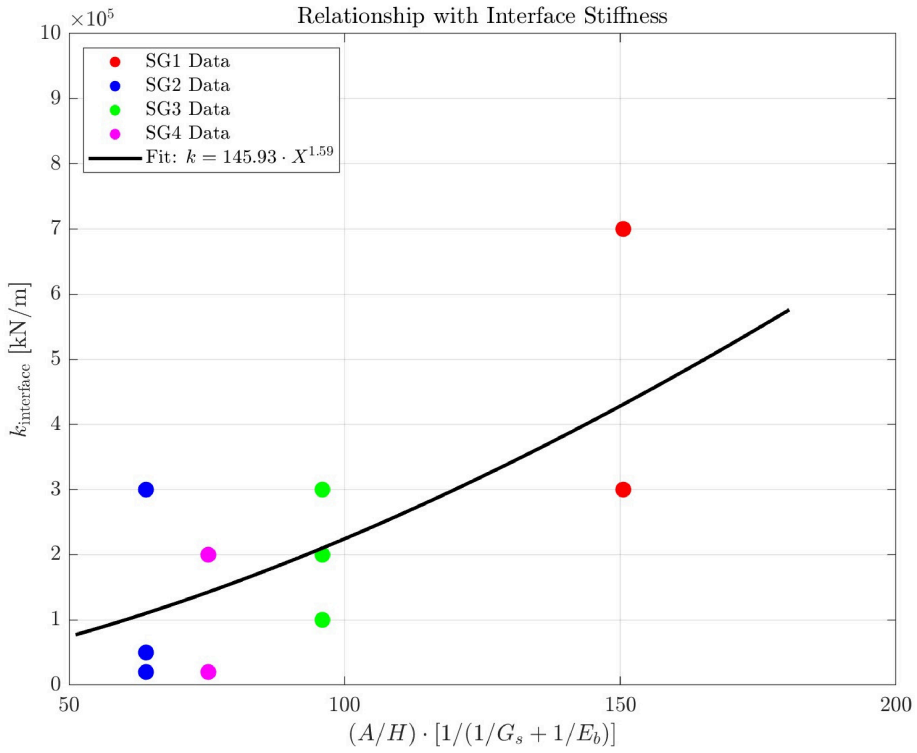


Figure 9. Empirical formulation of interface stiffness.

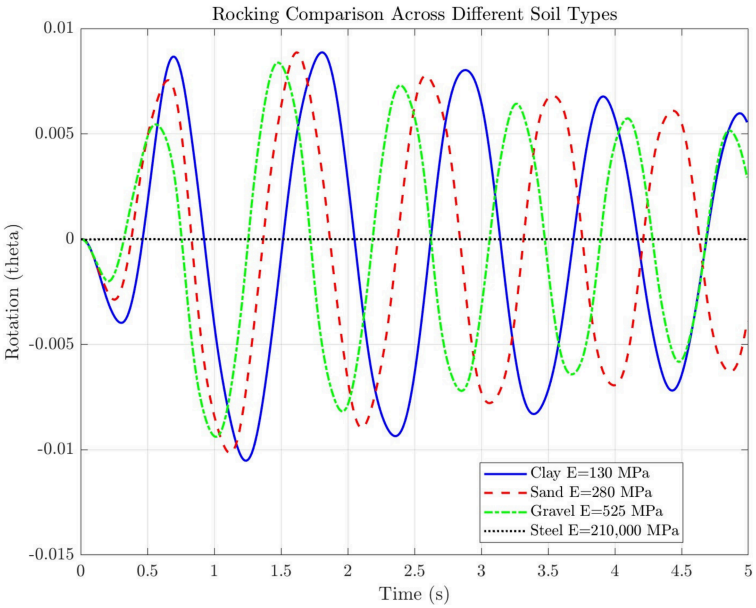


Figure 10. Rocking response over time for a rigid block R = 9.39, α = 0.44. on four types of soil: sand (solid blue), clay (dashed red), gravel (dash–dot green), and silt (dotted black).

5.2. Influence of Block Elastic Modulus E_b

The influence of the block's Young's modulus on the rocking motion, as depicted in Figure 11 varies across different soil types (clay, sand, gravel, and steel). The graphs compare the rotational response of a steel block and a concrete block under identical cosine excitation conditions on each soil type.

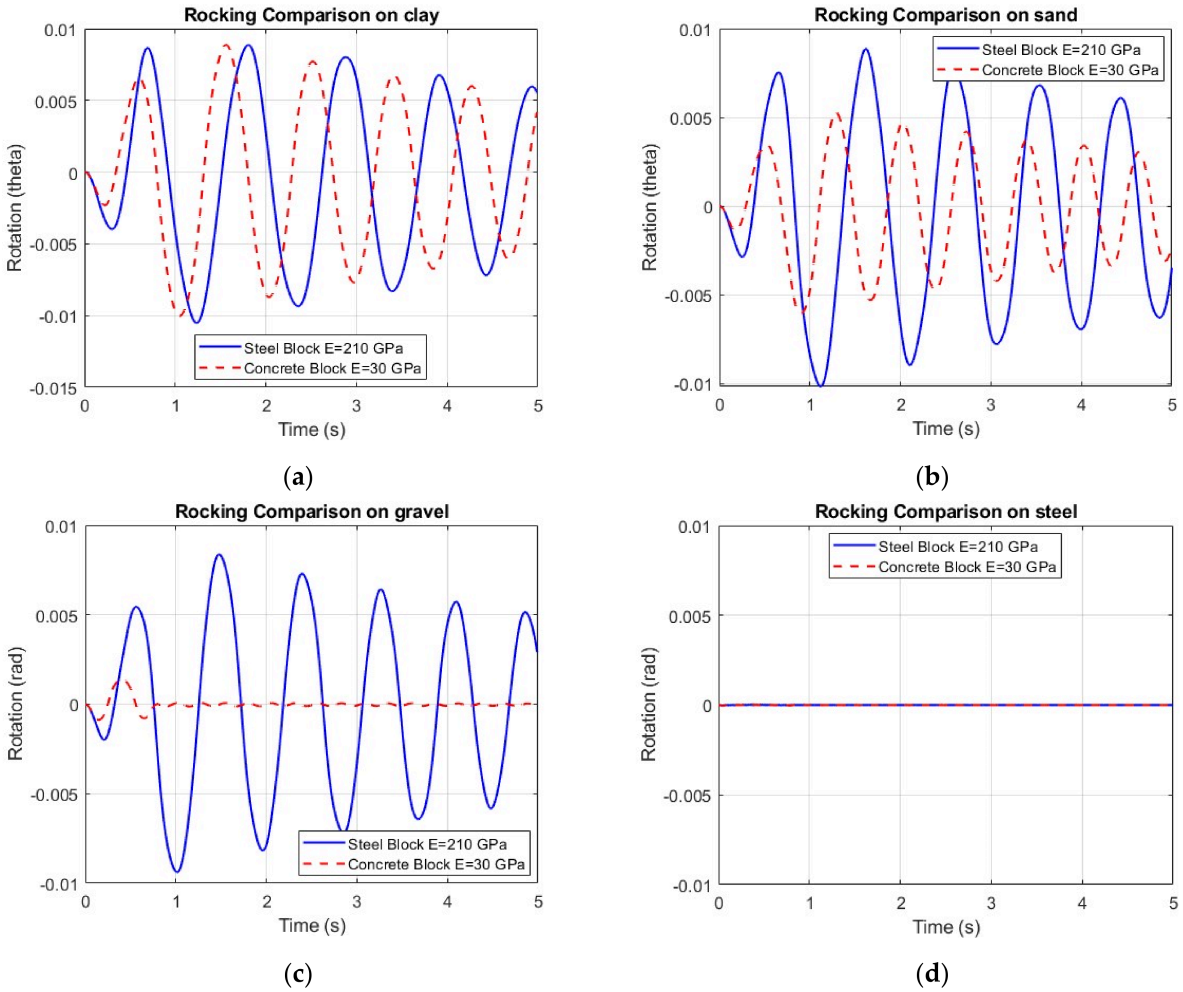


Figure 11. Comparison of rocking response over time for steel and concrete blocks on clay E = 130 MPa (**a**), sand $E = 280$ MPa (**b**), gravel $E = 525$ MPa (**c**), steel $E = 210,000$ MPa (**d**).

For softer soils like clay and sand, the block's E–modulus has a noticeable but relatively modest effect on the rocking motion. The steel and concrete blocks exhibit the same rocking amplitudes, while the rocking period of steel block compared to the concrete block increased slightly, indicating that a higher E–modulus (stiffer block) marginally enlarges the rocking period on a compliant base. On gravel, the difference becomes more pronounced. The rocking motion of steel block on gravel is considerably larger than the concrete block on gravel. On a very stiff base like steel, the rocking motion is heavily suppressed for both blocks, the cosine excitation was not strong enough to induce rocking. Overall, a higher block E–modulus (e.g., steel) tends to increase the amplitude and duration of rocking motion on a compliant base.

6. Conclusions

In conclusion, this study provides key insights into the behavior of rocking structures on softer subsoil bases, with the following points:

- The condition for rocking initiation is significantly altered on compliant bases, particularly when the subsoil stiffness is lower than that of competent rock, rendering the classical Housner rigid–block model inadequate for such scenarios.
- The applicability of Housner's model is restricted to substrates with a Young's modulus exceeding approximately 1000 MPa (consistent with rock–like bases).

Below this threshold, the model fails to accurately predict rocking response on compliant foundations.

- A novel soil–structure interaction (SSI) rocking model, accounting for structural rocking on a compliant base, was developed using Lagrange's formulation. The contact force within the model is characterized by an event–driven spring–dashpot system. To validate the framework, various structural geometries and ground motion records were employed. The proposed model demonstrates high fidelity when benchmarked against LS–DYNA simulations and Frost's compliant base model, exhibiting significant accuracy in predicting rocking responses on flexible foundations.
- An empirical formulation for interface stiffness was developed to calibrate the SSI–rocking model, ensuring its alignment with physical observations and enhancing its applicability to industrial design practice. Furthermore, this formulation significantly improves computational efficiency compared to complex experimental simulations, providing a high–speed alternative for analyzing rocking response during seismic events.

While the current research is limited by an elastic and one–layer soil profile, future research should evaluate the SSI–rocking model across a broader spectrum of geotechnical profiles, including cohesive soils and multi–layers, and diverse structural configurations. Extensive parametric analyses would facilitate an assessment of the model's robustness under varying seismic loading scenarios. Such efforts are essential for the potential development of standardized design guidelines for structural rocking on compliant foundations.

Author Contributions: Writing—original draft, Visualization, Validation, Software, Methodology, Formal analysis, Data curation, Conceptualization, Investigation. B.Y.; Writing—review and editing, Investigation, M.K.; Writing—review and editing, Investigation, H.S.-A. All authors have read and agreed to the published version of the manuscript.

Funding: This work was financially supported by the Deutsch Zentrum und Luft—und Raumfahrt (DLR), grant number IGF 22029 N.

Institutional Review Board Statement: Not applicable.

Informed Consent Statement: Not applicable.

Data Availability Statement: The data presented in this study are available on request from this corresponding author due to privacy.

Acknowledgments: The authors would like to acknowledge the use of DeepL Write (https://www.deepl.com/en/write) and Gemini 3.5 Flash (Google) for linguistic editing and structural refinement of this manuscript. These tools were utilized solely to enhance the clarity and readability of the text; all technical content, original derivations, and concluding interpretations remain the sole responsibility of the authors.

Conflicts of Interest: The authors declare that they have no known competing financial interests. Mrs. Mirjam Kloos is the employee of KOCH Solution Gmbh. The paper reflects the views of the scientists and not the company.

References

1. Groß, M.K.N.; Sadegh-Azar, H. Damping approaches in nonlinear seismic time history analysis for large mobile equipment with uplift. *Steel Constr.* **2023**, *17*, 119–129. [CrossRef]
2. Groß, M.; Gaube, D.; Sadegh, H. Grundsätzliche Untersuchungen zum seismischen Verhalten schienengebundener mobiler Großgeräte der Fördertechnik Teil 2: Seismische Analysen und Validierung. *Stahlbau* **2021**, *90*, 368–377. [CrossRef]
3. Groß, M.; Gaube, D.; Sadegh, H. Grundsätzliche Untersuchungen zum seismischen Verhalten schienengebundener mobiler Großgeräte der Fördertechnik Teil 1: Stand der Technik und Berechnungsansätze. *Stahlbau* **2021**, *90*, 169–178. [CrossRef]

4. Housner, G.W. The behavior of inverted pendulum structures during earthquakes. *Bull. Seism. Soc. Am.* **1963**, *53*, 403–417. [CrossRef]
5. Yim, C.; Chopra, A.K.; Penzien, J. Rocking response of rigid blocks to earthquakes. *Earthq. Eng. Struct. Dyn.* **1980**, *8*, 565–587. [CrossRef]
6. Zhang, J.; Makris, N. Rocking Response of Free-Standing Blocks under Cycloidal Pulses. *J. Eng. Mech.* **2001**, *127*, 473–483. [CrossRef]
7. ElGawady, M.A.; Ma, Q.; Butterworth, J.W.; Ingham, J. Effects of interface material on the performance of free rocking blocks. *Earthq. Eng. Struct. Dyn.* **2010**, *40*, 375–392. [CrossRef]
8. Dimitrakopoulos, E.G.; DeJong, M.J. Overturning of Retrofitted Rocking Structures under Pulse-Type Excitations. *J. Eng. Mech.* **2012**, *138*, 963–972. [CrossRef]
9. DeJong, M.J.; Dimitrakopoulos, E.G. Dynamically equivalent rocking structures. *Earthq. Eng. Struct. Dyn.* **2014**, *43*, 1543–1563. [CrossRef]
10. Vassiliou, M.F.; Makris, N. Estimating Time Scales and Length Scales in Pulselike Earthquake Acceleration Records with Wavelet Analysis. *Bull. Seism. Soc. Am.* **2011**, *101*, 596–618. [CrossRef]
11. Vassiliou, M.F.; Mackie, K.R.; Stojadinovic, B. A finite element model for seismic response analysis of deformable rocking frames. *Earthq. Eng. Struct. Dyn.* **2016**, *46*, 447–466. [CrossRef]
12. Vassiliou, M.F.; Truniger, R.; Stojadinović, B. An analytical model of a deformable cantilever structure rocking on a rigid surface: Development and verification. *Earthq. Eng. Struct. Dyn.* **2015**, *44*, 2775–2794. [CrossRef]
13. Bachmann, J.; Vassiliou, M.; Stojadinović, B. Dynamics of rocking podium structures. *Earthq. Eng. Struct. Dyn.* **2017**, *46*, 2499–2517. [CrossRef]
14. Bachmann, J.A.; Vassiliou, M.F.; Stojadinovic, B. Rolling and rocking of rigid uplifting structures. *Earthq. Eng. Struct. Dyn.* **2019**, *48*, 1556–1574. [CrossRef]
15. Bachmann, J.A.; Strand, M.; Vassiliou, M.F.; Broccardo, M.; Stojadinović, B. Is rocking motion predictable? *Earthq. Eng. Struct. Dyn.* **2017**, *47*, 535–552. [CrossRef]
16. Lachanas, C.G.; Vamvatsikos, D.; Vassiliou, M.F. The influence of the vertical component of ground motion on the probabilistic treatment of the rocking response of free-standing blocks. *Earthq. Eng. Struct. Dyn.* **2022**, *51*, 1874–1894. [CrossRef]
17. Manzo, N.R.; Lachanas, C.G.; Vassiliou, M.F.; Vamvatsikos, D. Uniform risk spectra for rocking structures. *Earthq. Eng. Struct. Dyn.* **2022**, *51*, 2610–2626. [CrossRef]
18. Manzo, N.R.; Vassiliou, M.F. Displacement-based analysis and design of rocking structures. *Earthq. Eng. Struct. Dyn.* **2019**, *48*, 1613–1629. [CrossRef]
19. Sieber, M.; Vassiliou, M.F.; Anastasopoulos, I. Intensity measures, fragility analysis and dimensionality reduction of rocking under far-field ground motions. *Earthq. Eng. Struct. Dyn.* **2022**, *51*, 3639–3657. [CrossRef]
20. Kazantzi, A.K.; Lachanas, C.G.; Vamvatsikos, D. Seismic response distribution expressions for on-ground rigid rocking blocks under ordinary ground motions. *Earthq. Eng. Struct. Dyn.* **2021**, *50*, 3311–3331. [CrossRef]
21. Lachanas, C.G.; Vamvatsikos, D.; Dimitrakopoulos, E.G. Statistical property parameterization of simple rocking block response. *Earthq. Eng. Struct. Dyn.* **2022**, *52*, 394–414. [CrossRef]
22. Lachanas, C.G.; Vamvatsikos, D. Rocking incremental dynamic analysis. *Earthq. Eng. Struct. Dyn.* **2021**, *51*, 688–703. [CrossRef]
23. Palmeri, A.; Makris, N. Response analysis of rigid structures rocking on viscoelastic foundation. *Earthq. Eng. Struct. Dyn.* **2008**, *37*, 1039–1063. [CrossRef]
24. Vassiliou, M.F.; Makris, N. Analysis of the rocking response of rigid blocks standing free on a seismically isolated base. *Earthq. Eng. Struct. Dyn.* **2011**, *41*, 177–196. [CrossRef]
25. Pelekis, I.; Madabhushi, G.S.; DeJong, M.J. Soil behaviour beneath buildings with structural and foundation rocking. *Soil Dyn. Earthq. Eng.* **2019**, *123*, 48–63. [CrossRef]
26. Pelekis, I.; Madabhushi, G.S.P.; DeJong, M.J. Seismic performance of buildings with structural and foundation rocking in centrifuge testing. *Earthq. Eng. Struct. Dyn.* **2018**, *47*, 2390–2409. [CrossRef]
27. Lu, Y.; Xiong, F.; Ge, Q. Dynamic rocking response of a rigid planar block on a nonlinear hysteretic Winkler foundation. *Earthq. Eng. Struct. Dyn.* **2021**, *50*, 2754–2773. [CrossRef]
28. He, D.; Li, P.; Zhang, Z. Analysis of a Simplified Model of a Rigid Rocking Block on Winkler Foundation. *Sustainability* **2023**, *15*, 5095. [CrossRef]
29. Frost, P.; Cacciola, P. Rocking of rigid blocks standing on a horizontally-moving compliant base. *Int. J. Non-Linear Mech.* **2023**, *153*, 104416. [CrossRef]
30. Li, Q.; Sun, X.; Zandi, Y.; Agdas, A.S.; Ali, H.E. Seismic response of submerged concrete structures under coupled nonlinear soil water and soil structure interaction. *Structures* **2026**, *87*, 111564. [CrossRef]
31. Rasa, A.Y.; Budak, A. Soil-structure-trench interaction effects on vibration isolation of multi-story structures. *J. Braz. Soc. Mech. Sci. Eng.* **2026**, *48*, 186. [CrossRef]

32. Feng, J.; Zhou, L.; Nie, F.; Hua, J.; Li, Y. Investigation on the dynamic fracture behavior of three-centered circle twin tunnels containing a joint under impact loading. *Theor. Appl. Fract. Mech.* **2025**, *139*, 105010. [CrossRef]
33. Baugrunddynamik, A. *Empfehlungen des Arbeitskreises Baugrunddynamik*; Herausgegeben von der Deutschen Gesellschaft für Geotechnik e.V. (DGGT): Essen, Germany, 2019.

Disclaimer/Publisher's Note: The statements, opinions and data contained in all publications are solely those of the individual author(s) and contributor(s) and not of MDPI and/or the editor(s). MDPI and/or the editor(s) disclaim responsibility for any injury to people or property resulting from any ideas, methods, instructions or products referred to in the content.